Investigating Molecular Kinetics by Variationally Optimized Diffusion Maps

Lorenzo Boninsegna,[†] Gianpaolo Gobbo,[‡] Frank Noé,[*,¶] and Cecilia Clementi[*,†]

Rice University, Center for Theoretical Biological Physics and Department of Chemistry, 6100 Main St, Houston, TX 77005, USA , Maxwell Institute for Mathematical Sciences and School of Mathematics, The University of Edinburgh, Peter Guthrie Tait Road, Edinburgh EH9 3FD, United Kingdom, and FU Berlin, Department of Mathematics, Computer Science and Bioinformatics, Arnimallee 6, 14195 Berlin, Germany

E-mail: frank.noe@fu-berlin.de; cecilia@rice.edu

Abstract

Identification of the collective coordinates that describe rare events in complex molecular transitions such as protein folding has been a key challenge in the theoretical molecular sciences. In the diffusion map approach, one assumes that the molecular configurations sampled have been generated by a diffusion process, and one uses the eigenfunctions of the corresponding diffusion operator as reaction coordinates. While diffusion coordinates appear to provide a good approximation to the true dynamical reaction coordinates, they are not parametrized using dynamical information. Thus,

[*]To whom correspondence should be addressed

[†]Rice University, Center for Theoretical Biological Physics and Department of Chemistry, 6100 Main St, Houston, TX 77005, USA

[‡]Maxwell Institute for Mathematical Sciences and School of Mathematics, The University of Edinburgh, Peter Guthrie Tait Road, Edinburgh EH9 3FD, United Kingdom

[¶]FU Berlin, Department of Mathematics, Computer Science and Bioinformatics, Arnimallee 6, 14195 Berlin, Germany

their approximation quality could as yet not been validated, neither could the diffusion map eigenvalues be used to compute relaxation rate constants of the system. Here we combine the diffusion map approach with the recently proposed variational approach for conformation dynamics (VAC). Diffusion maps coordinates are used as a basis set, and their optimal linear combination is sought using the VAC that employs time-correlation information of the molecular dynamics (MD) trajectories. We have applied this approach to ultra-long MD simulations of the Fip35 WW domain and found that the first diffusion coordinates are indeed a good approximation to the true reaction coordinates of the system but they could be further improved using the VAC. Using the diffusion map basis, excellent approximations to the relaxation rates of the system are obtained. Finally we evaluate the quality of different metric spaces, and find that pairwise minimal root mean square deviation (RMSD) performs poorly, while operating in the recently introduced kinetic maps based on the time-lagged independent component analysis performs best.

Introduction

Molecular dynamics (MD) simulations have now reached considerable maturity. A few years ago, extensive sampling of protein systems was still unfeasible - except in a few exceptional projects such as folding@home[1] or the Anton supercomputer.[2] Now, it is commonly possible to achieve hundreds of microseconds of cumulative simulation time by harvesting the computational power of GPU's,[3–5] thus enabling extensive sampling of many biomolecular processes at moderate cost.

With the ability to generate vast amounts of molecular dynamics data on a broad scale, analyzing these data and interpreting them in physicochemically relevant models has become a bottleneck. Consequently, the last years have seen a surge of interest in kinetic models that describe both the equilibrium behavior as well as the transition dynamics amongst a set of discrete conformational states. Popular examples include Markov models or Markov

states models (MSMs),[6–12] hidden Markov models (HMMs),[13,14] diffusion maps,[15,16] transition networks,[17–19] and Langevin models.[20] All of these models aim at achieving a simplified and interpretable, yet accurate picture of the dynamics observed in the available MD trajectories. The questions of interest include: which are the most relevant long-lived states or structures of the molecular system[9,14,21–24]? What are their probabilities, transition rates and relaxation timescales[11,25–27]? What are the transition pathways or mechanisms leading from reactants such as the unfolded or dissociated state to products such as the folded or associated states[28–33]?

It has been realized[6] that the most interesting quantities containing information of both the equilibrium and the slow kinetic properties of a molecular system are the dominant eigenvalues and eigenfunctions of the Markov operator. The eigenfunctions are typically nearly constant on the long-lived (metastable) states, but they change their sign between those regions. In this way, they encode parts of the state space where the system generally remains for a long time, and it rarely transitions between them. This concept is known as metastability and is a typical feature of biomolecules. The metastable regions of state space are frequently associated with biological function of the molecule, e.g. the ability / inability to bind to a binding partner. Therefore, it is precisely these regions that we are most interested in. The eigenvalues on the other hand, contain the information about the time it takes until such a rare transition might occur.

Indeed many quantities of interest can be computed given an approximation of the eigenvalues and eigenfunctions, including metastable states,[6,9,14,21] coarse-grained Markov models[34] and experimentally measurable observables.[27,35] Having obtained the eigenfunctions, these can serve to define optimal reaction coordinates[33,36,37] and even simulation methods that are efficient in sampling the rare events.[38,39] Most of the molecular kinetics models above directly aim at, or can be shown to effectively attempt to, reconstruct or approximate these eigenvalues and eigenfunctions.[15,16,40]

Since it was realized that the quality of the molecular kinetics model crucially depends

on its ability to approximate the dominant eigenfunctions,[15,25,40] substantial research has gone into attempting to improve this approximation. Two developments are particularly noteworthy: Firstly, the time-lagged (or time-structured) independent component analysis (TICA)[41–43] conducts a linear transformation of the molecular coordinates (e.g. internal coordinates such as distances or angles) onto a maximally slow subspace. It can be shown[42] that this method provides the optimal linear subspace for representing the eigenfunctions of the dynamical system, and thus a very good starting point for constructing a Markov model or other kinetics models that further improve the approximation of the eigenvectors. Secondly, diffusion maps[15] and particularly locally scaled diffusion maps[16] attempt to construct a direct approximation of the same set of eigenfuctions by nonlinearly projecting the high dimensional configuration space onto a low dimensional hyperplane spanned by the dominant eigenfunctions to be approximated. In principle, diffusion maps allow a much better approximation to the Markov operator eigenfunctions than a cluster discretization of state space, because they can operate on each sample configuration.

Despite these nice properties, a major drawback of diffusion maps has been that they are purely based on the idea that the spatial distribution of sampled configurations has been generated by a diffusion process. The construction of eigenfunction approximations through diffusion maps goes thus through the assumption of a specific dynamical model *a priori* (namely, a Fokker-Planck diffusion), and not through actual parametrization of dynamical observables in the data. As a consequence, diffusion maps currently have two drawbacks: (1) The validity of diffusion coordinates as eigenfunction approximants cannot be self-consistently checked within the diffusion map framework, and their approximation quality cannot be improved; (2) The diffusion map eigenvalues cannot be directly related to physically meaningful relaxation timescales.

Here we set out to solve these two problems. Recently, one of the authors has contributed to develop a variational principle and the variational approach for conformation dynamics (VAC).[44,45] In brief, this theory makes two statements:

1. Many molecular kinetics models, including MSMs, can be understood as attempting to approximate the eigenfunctions of the Markov operator by a linear combination of basis functions. The approximation is exact if the eigenvalue is approximated exactly as well. While the approximation is suboptimal, the estimated eigenvalue will be too small. This idea can be cast into a rigorous variational formulation.

2. Inspired by the analogy with Quantum Mechanics, a method of linear variation can be formulated which maximizes the estimation of the dominant eigenvalues in order to systematically exploit the variational bound. This is easily achieved by proposing a set of basis functions, building their linear combinations and varying the coefficients till the optimal solution is found. The optimized linear combinations are then approximations of the dominant eigenvectors.

Here we exploit the variational principle and the algorithmic idea to validate and variationally optimize diffusion coordinates. The main idea is that coordinates obtained by the locally scaled diffusion map method[16] are already a good approximation to the true eigenfunctions of the dynamical operator. We then use the dominant diffusion coordinates in order to define a basis set that we further optimize using the method of linear variation. As a result, we get an improved approximation of the eigenfunctions and additionally we get eigenvalues that can be interpreted as physical relaxation timescales. The resulting method is called variationally optimized diffusion map (varDM), and overcomes both diffusion map issues discussed before.

We describe the theory and methodology and apply the varDM method to analyze two all-atom 100 μs Fip35 WW domain trajectories generated by the special purpose Anton supercomputer.[2] This data has been previously analyzed using a number of other methods,[2,46–50] and it provides an ideal benchmark for our approach.

The manuscript is organized as follows. After briefly introducing the operators implementing the dynamics and discussing why their eigenvectors and eigenvalues are relevant in the context of molecular dynamics and simulations, we describe how they can be approx-

imated from a simulation dataset, specifically focusing on the Method of Linear Variation and the Locally Scaled Diffusion Map. Particular attention will be devoted to discussing how the concept of distance can play a crucial role in the diffusion map definition. Results for independent VarDM calculations for different setups are compared and contrasted, together with a benchmark MSM calculation. The results show that standard (purely structurally based) protocols to compute distances between molecular configurations are inadequate at approximating higher order dominant eigenprocesses. In contrast, a kinetic distance based on the TICA dimensionality reduction procedure provides an optimal definition of distance for the construction of diffusion maps. The molecular mechanisms associated with the data are then interpreted and discussed, in comparison with previous studies.

Theory

Conformation dynamics, eigenfunctions and eigenvalues

A molecular dynamics (MD) simulation can be described as a Markov Process in a state space Ω (generally containing both positions and momenta) that samples from an equilibrium probability density π. π is, for our purposes, given by the Boltzmann distribution at a constant temperature T:

$$\pi(\mathbf{x}) \quad = \quad Z^{-1}\mathrm{e}^{-\beta U(\mathbf{x})},$$

where $\beta = (k_B T)^{-1}$ is the inverse temperature, $U(\mathbf{x})$ is the potential energy at phase space point $\mathbf{x}$, and Z is the partition function.

Next, a formal way of describing the dynamics has to be introduced. We would like to stay as generic as possible and only state a few general properties that our dynamics must fulfill, without focusing on any specific model. Firstly, the dynamics should be Markovian in full phase space, i.e. there is a probability density $p_\tau(\mathbf{y} \mid \mathbf{x})$ of making a transition, that

is, to find the system at state $\mathbf{y}$ at a later time $t + \tau$ during the MD trajectory, given that it was at state $\mathbf{x}$ at time t. Many of the choices that can be made in a molecular dynamics program, such as the thermostat and integrator used, will affect $p_\tau(\mathbf{y} \mid \mathbf{x})$ and will therefore also affect the kinetics, i.e. the transition rates between different conformations. However, independently of the specific choice of the dynamics, we require $p_\tau(\mathbf{y} \mid \mathbf{x})$ to have the following two properties:

- The dynamics are ergodic, i.e. if we run them long enough ($\tau \to \infty$), $p_\tau(\mathbf{y} \mid \mathbf{x})$ will sample from the Boltzmann density $\pi(\mathbf{x})$.
- The dynamics satisfy detailed balance:

$$\pi(\mathbf{x})\, p_\tau(\mathbf{y} \mid \mathbf{x}) \;\; = \;\; \pi(\mathbf{y})\, p_\tau(\mathbf{x} \mid \mathbf{y})\, \forall \mathbf{x}, \mathbf{y} \in \Omega, \tag{1}$$

Physically, eq. (1) is consistent with the second law of thermodynamics in its formulation that work cannot be produced from thermal energy alone. Unfortunately not every implementation of molecular dynamics obeys eq. (1). It turns out that we can still work with dynamics implementations that fulfill a generalized form of detailed balance, where forward and backward probabilities are equal when momenta are reversed.[51] Langevin dynamics is an example of such a dynamics with generalized detailed balance. In this case (1) can be restored at the cost of Markovianity if x is in position space and momenta are integrated out. Nonetheless, since typical τ values are far larger than the autocorrelation times of momenta, the dynamics are still very closely Markovian in position space at timescale τ such that the present theoretical picture is conceptually useful. For the sake of simplicity, we will just assume for the subsequent discussion that eq. (1) is fulfilled.

We now introduce a propagator formulation of such an ergodic and Markovian dynamics following the discussion given in.[45] Using the state space function ρ_t, we can formally write

the action of the molecular dynamics in terms of a propagator:

$$\rho_{t+\tau} = \mathcal{P}(\tau) \circ \rho_t$$

where ρ_t quantifies the instantaneous probability density at time t. i.e., ρ_t measures for an ensemble of copies of a molecular system what fraction of its population is in which conformation. The propagator $\mathcal{P}$ propagates this density in time. Given the above requirements, it is obvious that after sufficiently many applications of $\mathcal{P}$, or for a long enough time τ, the resulting density will just be the equilibrium density $\pi(\mathbf{x})$. Table (1) defines $\mathcal{P}$ as a function of $p_\tau(\mathbf{y} \mid \mathbf{x})$. Note that we will never explicitly compute $\mathcal{P}$ or carry out the integrals in Table (1). However, we know that when running MD simulations, we effectively sample these integrals, and this gives us a way to construct a model for $\mathcal{P}$ and through that for the most interesting kinetic quantities.

Although it may seem like a purely mathematical comment, it is sometimes convenient or even necessary to work with a different operator than $\mathcal{P}$.[45] It is then appropriate to define the relative density u_t by:

$$u_t(\mathbf{x}) = \frac{\rho_t(\mathbf{x})}{\pi(\mathbf{x})}, \tag{2}$$

which is obtained by comparing the instantaneous density with the stationary density. Instead of working with $\mathcal{P}$ we can work with the transfer operator $\mathcal{T}(\tau)$ that transports u-densities in time:

$$u_{t+\tau} = \mathcal{T}(\tau) \circ u_t$$

When $\rho_t(\mathbf{x})$ is identical to the equilibrium density, it follows from the definition (2) that the relative density is identical to 1. Table (1) summarizes the properties of both operators.

It turns out that both the $\mathcal{P}(\tau)$ and $\mathcal{T}(\tau)$ operators are of great interest. The eigenfunctions and eigenvalues of these operators contain the essential information of the molecular

Table 1: Overview of dynamical operators for describing conformation dynamics and their spectral expansions.

	Propagator	Transfer operator
Symbol	$\mathcal{P}(\tau)$	$\mathcal{T}(\tau)$
Definition	$\mathcal{P}(\tau) \circ \rho(\mathbf{x})$ $= \int_{\mathbf{x}\in\Omega} \rho(\mathbf{x})\, p_\tau(\mathbf{y} \mid \mathbf{x})\, d\mathbf{x}$	$\mathcal{T}(\tau) \circ u(\mathbf{y})$ $= \frac{1}{\pi(\mathbf{y})} \int_{\mathbf{x}\in\Omega} \pi(\mathbf{x})\, u(\mathbf{x})\, p_\tau(\mathbf{y} \mid \mathbf{x})\, d\mathbf{x}$
Scalar product	$\langle f, g\rangle_{\pi^{-1}}$ $= \int_{\mathbf{x}\in\Omega} \frac{1}{\pi(\mathbf{x})} f(\mathbf{x})g(\mathbf{x})\, d\mathbf{x}$	$\langle f, g\rangle_{\pi}$ $= \int_{\mathbf{x}\in\Omega} \pi(\mathbf{x}) f(\mathbf{x})g(\mathbf{x})\, d\mathbf{x}$
Eigenfunctions	$\phi(\mathbf{x}) = \pi(\mathbf{x}) \cdot \psi(\mathbf{x})$	$\psi(\mathbf{x}) = \pi^{-1}(\mathbf{x}) \cdot \phi(\mathbf{x})$
Spectral expansion	$\mathcal{P}(\tau) \circ \rho(\mathbf{x})$ $= \sum_{k=0}^{\infty} e^{-\kappa_k \tau} \langle \phi_k, \rho\rangle_{\pi^{-1}} \phi_k$	$\mathcal{T}(\tau) \circ u(\mathbf{y})$ $= \sum_{k=1}^{\infty} e^{-\kappa_k \tau} \langle \psi_k, u\rangle_{\pi} \psi_k$
Truncated expansion	$\mathcal{P}(\tau) \circ \rho(\mathbf{x})$ $\approx \sum_{k=1}^{m} e^{-\kappa_k \tau} \langle \phi_k, \rho\rangle_{\pi^{-1}} \phi_k$	$\mathcal{T}(\tau) \circ u(\mathbf{y})$ $\approx \sum_{k=0}^{m} e^{-\kappa_k \tau} \langle \psi_k, u\rangle_{\pi} \psi_k$
Stationary density	$\phi_0(\mathbf{x}) = \pi(\mathbf{x}) = \mathrm{e}^{-\beta U(\mathbf{x})}$ (Boltzmann density)	$\psi_0(\mathbf{x}) = 1$
Corresp. Generator	Forward Generator $\mathcal{L}$ $\mathcal{P}(\tau) = \exp(\tau\mathcal{L})$	Backward Generator $\mathcal{L}^*$ $\mathcal{T}(\tau) = \exp(\tau\mathcal{L}^*)$

kinetics, i.e. what are the long-lived states and what are the transition rates between them. Understanding the mathematical properties of these operators allows to design computational methods to approximate their spectra and thus chemically interesting quantities. A plethora of different methods such as Markov models, diffusion maps, the variational principle of conformational dynamics (and many more) are based on this idea.

Both $\mathcal{P}$ and $\mathcal{T}$ operators share the same eigenvalues. The largest eigenvalue is $\lambda_0 = 1$, whereas all remaining eigenvalues are strictly smaller than one:

$$1 = \lambda_0 > \lambda_1 \geq \cdots$$

The eigenfunction corresponding to the largest eigenvalue $\lambda_0 = 1$ is just the stationary Boltzmann density for the propagator and the constant function for the transfer operator. All eigenvalues except the first decay exponentially with the lag-time τ, i.e. we have

$$\lambda_k(\tau) \;=\; e^{-\kappa_k \tau} \tag{3}$$

with some relaxation rates κ_k. Thus, knowing the eigenvalues allows us to compute the relaxation rates, or the relaxation timescales:

$$t_k \quad = \kappa_k^{-1} = \quad -\frac{\tau}{\log|\lambda_k(\tau)|}. \tag{4}$$

These relaxation rates or timescales are important quantities to compare to experiments, as they directly affect the measurement signal in various kinetic experiments such as fluorescence correlation spectroscopy,[27] 2D IR spectroscopy,[52] temperature jump spectroscopy,[30] neutron scattering[53] (a comprehensive review can be found in Keller *et al.*[35]).

The eigenfunctions ϕ or ψ are the key quantities for understanding molecular mechanisms. It was proposed in[6] that the different metastable (long-lived) states of a molecule could be identified by sorting its microstates according to the signs they have in the eigenfunctions corresponding to the slowest relaxations, i.e. those with the largest eigenvalues. This idea was further refined in.[54] In Noé *et al.*[27] it was used in order to construct a systematic way of giving a structural interpretation to ensemble kinetics experiments with the help of molecular dynamics simulations. Both Markov state models and diffusion map algorithms attempt to approximate the eigenfunctions ϕ or ψ. It was found that the accuracy by which these eigenfunctions are approximated is crucial for the accuracy of the model.[25,40]

When studying molecular kinetics we are usually interested in the slow processes only. Therefore, for a sufficiently large choice of τ (e.g. in the order of nanoseconds), only a finite number m of the terms in the spectral expansion are still present, and the operator's action can be understood in terms of only finitely many processes, and we obtain the truncated expansions shown in Table (1). We are then interested in methods that allow us to compute (or approximate) a few dominant eigenvalues $\lambda_1, ..., \lambda_m$ and their corresponding eigenfunctions $\phi_1, ..., \phi_m$. Alternatively we may also work with $\psi_1, ..., \psi_m$ provided that some estimate of the equilibrium distribution π is available.

Method of linear variation and the special variational principle

A number of useful computational methods have been developed in the last years to approximate the eigenvalues and eigenfunctions of the propagator or transfer operator. Recently, a very general approximation principle for such purpose was proposed: the variational principle of conformation dynamics.[45] Briefly, if f is some approximation model of the first non trivial $\mathcal{T}(\tau)$ eigenfunction, $f \approx \psi_1$, then the Rayleigh-Quotient

$$\hat{\lambda}_1(\tau) \quad = \quad \frac{\langle f, \mathcal{T}(\tau) f \rangle_\pi}{\langle f, f \rangle_\pi} \tag{5}$$

is an estimate to the corresponding eigenvalue $\hat{\lambda}_1(\tau) \approx \lambda_1(\tau)$ (please see Table (1) for the definition of the scalar product) The variational principle states that $\hat{\lambda}_1$ always underestimates the true eigenvalue ($\hat{\lambda}_1(\tau) \leq \lambda_1(\tau)$), equivalence holding only if $f = \psi_1$. If f is an approximation to other eigenfunctions ($\psi_2, ...$) and constructed such that it is orthogonal to previous exact eigenfunctions ($\psi_0 = 1, \psi_1, ...$), then this variational principle also carries over to subsequent eigenvalue/eigenfunction pairs. Thus, a computational algorithm can approximate eigenvalue/eigenfunction pairs by proposing a model for the eigenfunction and then optimizing it by maximizing the corresponding Rayleigh coefficient.

From a practical perspective, the crucial insight from the VAC is that the Rayleigh coefficients can be easily computed for a given model function f in terms of its autocorrelation function.[45] Furthermore, the search for the optimal model can be performed in a single step if we consider eigenfunctions to be a weighted sum of basis functions $\{\chi_1(x), \ldots, \chi_N(x)\}$, i.e.:

$$\hat{\psi}_i(\mathbf{x}) = \sum_{j=1}^{m} a_{ij} \chi_j(\mathbf{x}). \tag{6}$$

In this case, the optimal solution consists of finding the optimal coefficients a_{ij} which are just given by applying the generalized Ritz (or Rothaan-Hall) method to conformation dynam-

ics.[45] One computes the correlation matrices $\mathbf{C}(\tau)$ and $\mathbf{C}(0)$ with elements:

$$c_{ij}(\tau) = \langle \chi_i, \mathcal{T}(\tau)\chi_j \rangle_\pi, \quad (7)$$

$$c_{ij}(0) = \langle \chi_i, \chi_j \rangle_\pi. \quad (8)$$

and obtains the optimal coefficients a_{ij} by solving the generalized eigenvalue problem:[44,45]

$$\mathbf{C}(\tau)\,\mathbf{a}_i = \hat{\lambda}_i \mathbf{C}(0)\,\mathbf{a}_i, \quad (9)$$

where $\mathbf{a}_i \in R^m$ is the vector of coefficients of the functions χ_i to build the i-th optimized linear combination. We refer to the Methods section for a description of how the correlation matrix elements (7-8) are actually computed from a MD trajectory. The generalized eigenvalue problem (9) occurs in other kinetic models and estimators, such as Markov models with fuzzy partitions of unity,[55] core- or milestoning-based MSMs,[26] time-lagged independent component analysis (TICA),[42] and ordinary MSMs that can all be treated as special cases of the variational approach of conformation dynamics with specific choices of basis sets (see[45] for a discussion).

When using the method of linear variation to compute eigenvalues and eigenvectors, we can derive a special variational principle that holds for the solutions of the eigenvalue problem (9):

1. If we use the exact eigenvectors 0 through m as basis functions $\chi_i = \psi_i$, we will obtain:

$$c_{ij}(0) = \langle \psi_i, \psi_j \rangle_\pi = \delta_{ij} \quad (10)$$

$$c_{ij}(\tau) = \langle \psi_i, \mathcal{T}(\tau)\psi_j \rangle_\pi = \delta_{ij}\lambda_i(\tau) \quad (11)$$

and thus:

$$\mathbf{C}(0) = \mathbf{Id} \tag{12}$$

$$\mathbf{C}(\tau) = \mathbf{\Lambda}(\tau) \tag{13}$$

so the eigenvalue problem becomes trivial and we recover the exact eigenvalues $\hat{\lambda}_i(\tau) = \lambda_i(\tau)$ for all $i = 1, ..., m$.

2. If we have a basis set error, i.e. the exact eigenvectors can *not* be represented as a linear combination of basis functions (6), then we have the following special variational constraint on the eigenvalues:

$$\hat{\lambda}_i(\tau) < \lambda_i(\tau) \quad \text{for all } i = 1, ..., m.$$

We have the variational principle for all m eigenvalues because our eigenvectors are by construction an orthogonal set of vectors.

3. The accuracy of the variational approach strictly depends on the choice of the basis functions.

(Locally Scaled) Diffusion Map and Diffusion Coordinates (DCs)

The Diffusion Map algorithm is an independent approach to approximate the transfer operator eigenfunctions ψ_i starting from an equilibrium MD dataset. The description of the algorithm and its ideas that we present here closely parallels that given by Coifman *et al.*[56]

In the diffusion map formalism we assume that the configurations in the sampling were generated by a specific dynamical model being pure diffusion in the potential $U(\mathbf{x})$ (from now on, $\mathbf{x}$ will denote a point in the configuration space). Then, the system dynamics is governed

by the Fokker-Planck equation:

$$\frac{\partial \rho}{\partial t} = \mathcal{L} \circ \rho = \frac{\Delta \rho}{\beta} + \nabla(\rho \nabla U) \tag{14}$$

where again $\rho(\mathbf{x})$ is the probability density of state $\mathbf{x}$, $\beta = (kT)^{-1}$ is the inverse temperature and the gradient ∇U is minus the drift (force) at position $\mathbf{x}$. The operator $\mathcal{L}$ is the diffusion generator and it is a differential operator that models the instantaneous time change of the state space density. It is yet another way of modeling the system's dynamics and it is related to the propagator $\mathcal{P}(\tau)$ by an exponentiation, i.e. $\mathcal{P}(\tau) = \exp(\tau\mathcal{L})$, see Table (1). $\mathcal{L}$ has a discrete spectrum with nonpositive eigenvalues $\{-\kappa_j\}_{j=0}^{\infty}$ where $\kappa_0 = 0 < \kappa_1 \leq \kappa_2 \leq ...$, are the system's relaxation rates of Eq. (3). $\mathcal{L}$ has associated eigenfunctions $\{\phi_j\}_{j=0}^{\infty}$ that are identical to the propagator eigenfunctions (see Table (1)). Like for propagators and transfer operators, we can write (at least formally) the solution of (14) as

$$\rho_{t+\tau}(\mathbf{y}) = \sum_{j=0}^{\infty} \langle \phi_i(\mathbf{x}) \mid \rho_t(\mathbf{x}) \rangle_{\pi^{-1}} \mathrm{e}^{-\kappa_i \tau} \phi_i(\mathbf{y}). \tag{15}$$

which in the limit of long τ converges to $\phi_0(\mathbf{x}) = \pi(\mathbf{x})$ corresponding to the eigenvalue $\kappa_0 = 0$, which is given by the Boltzmann equilibrium distribution.

A complementary approach is to use the backward Fokker-Planck equation which implements the time evolution of $\pi-$reduced probability densities

$$\frac{\partial u}{\partial t} = \mathcal{L}^* u = \frac{\Delta u}{\beta} - \nabla u \cdot \nabla U \tag{16}$$

The backward generator $\mathcal{L}^*$ has the same eigenvalues as operator $\mathcal{L}$ but the same eigenfunctions $\psi_i(x)$ as the transfer operator (see Table (1)). It is related to the transfer operator $\mathcal{T}$ by $\mathcal{T}(\tau) = \exp(\tau\mathcal{L}^*)$, see Table (1). A similar infinite decomposition as (15) can be written for the reduced u probability as well.

For any starting point $\mathbf{x} \in \Omega$, let $\rho_\tau(\mathbf{y} \mid \mathbf{x})$ be the solution of the forward Fokker-Planck equation with initial condition $\rho_0(\mathbf{x}) = \delta(\mathbf{x} - \mathbf{y})$. The diffusion distance between any of the two points $\mathbf{x}_1, \mathbf{x}_2 \in \Omega$ at time τ is defined as the distance between the corresponding probability densities at time τ, when initialized at $\mathbf{x}_1$ or at $\mathbf{x}_2$ at time 0.[56] The distance is measured in the Hilbert space $L_2(\Omega, w)$ with the weight function $w(\mathbf{x}) = 1/\varphi_0(\mathbf{x}) = \pi^{-1}(\mathbf{x})$. The distance can be written as

$$D_\tau^2(\mathbf{x}_1, \mathbf{x}_2) = ||\rho_{t+\tau}(\mathbf{y} \mid \mathbf{x}_1) - \rho_{t+\tau}(\mathbf{y} \mid \mathbf{x}_2)||_{\pi^{-1}}^2 \tag{17}$$

Using equation (15) and its relation with (16), we obtain the spectral representation

$$D_\tau^2(\mathbf{x}_1, \mathbf{x}_2) = \sum_{i \geq 1} e^{-2\kappa_i \tau} \left\| \psi_i(\mathbf{x}_1) - \psi_i(\mathbf{x}_2) \right\|^2 \tag{18}$$

Many times, molecular systems are metastable and their dynamics is dominated by a (finite) number m of slow processes encoding the more interesting physics, while all the other processes $m+1, \cdots$ decay much faster over time and encode more subtle, less crucial dynamical features. From a mathematical standpoint, this means that the propagator eigenvalues display a spectral gap at an index m, i.e. $\kappa_m \ll \kappa_{m+1}$. The infinite expansions above (18), (15) can then be truncated up to the m-th term, if only the slow regime is of interest

$$\rho_{t+\tau}(\mathbf{y}) = \phi_0(\mathbf{x}) + \sum_{j=1}^{m} \langle \phi_i(\mathbf{x}) \mid \rho_t(\mathbf{x}) \rangle_{\pi^{-1}} \mathrm{e}^{-\kappa_i \tau} \phi_i(\mathbf{y}). \tag{19}$$

The Diffusion Map algorithm can then be seen as the specific nonlinear mapping from the original high dimensional $\mathbf{x}$ configuration space to a m-th dimensional Euclidean space that preserves the diffusion distance between each pair of the points in the dataset.[15,16,56] The main result to be mentioned here is that the low dimensional representation space is spanned by the eigenvectors of the generator $\mathcal{L}$, which are automatically computed upon carrying out

the projection.

Now consider that we are given a sample of points, $\{\mathbf{x}_i\}_{i=1,\ldots,N}$ generated for example by a long molecular dynamics trajectory. The elementary steps of the diffusion map algorithm are the following:

1. Consider the kernel
$$K(\mathbf{x}_i, \mathbf{x}_j) = \exp\left(-\frac{\|\mathbf{x}_i - \mathbf{x}_j\|^2}{2\epsilon^2}\right) \tag{20}$$
where ϵ is a scale parameter. $||\cdots||$ denotes the distance between configurations $\mathbf{x_i}$ and $\mathbf{x}_j$. The Locally Scaled Diffusion Map (LSDMap) formulation[16] differs from the original Diffusion Map[15] in the definition of a local scale parameter $\epsilon(\mathbf{x})$ that is a function of the configuration $\mathbf{x}$, rather than a constant value ϵ. For reasons of symmetry, ϵ^2 in (20) is replaced by $\epsilon(\mathbf{x}_i)\epsilon(\mathbf{x}_j)$. The local scale has not been derived from a diffusion process in the input coordinate space, but is rather a model parameter that has practically proven to perform significantly better than a constant scale for the definition of reaction coordinates and in adaptive sampling schemes.[16,39] It is worth mentioning that the particular choice for both $||\cdots||$ and ϵ may severely affect the algorithm performance, as we will discuss later.

2. Normalize the kernel as
$$\tilde{K}_{i,j} = \frac{K(\mathbf{x}_i, \mathbf{x}_j)}{\sqrt{\sum_k K(\mathbf{x}_i, \mathbf{x}_k) \sum_k K(\mathbf{x}_j, \mathbf{x}_k)}} \tag{21}$$

3. Define $D_i = \sum_j \tilde{K}_{i,j}$, and construct the diffusion map transition matrix
$$M_{i,j} = \frac{\tilde{K}_{i,j}}{D_i} \tag{22}$$

4. Calculate the first m eigenvectors of M, $\{\tilde{\psi}_i\}$. Note that the eigenvectors $\tilde{\psi}_i$ are defined on the sampled configurations $\mathbf{x} \in \Omega$ pointwise.

The eigenvectors $\tilde{\psi}_i$ are called *diffusion coordinates* (DCs) and are point-wise approximations of the exact eigenvectors $\psi_i(x)$.

$$\tilde{\psi}_i(\mathbf{x}) = DC_i(\mathbf{x}) \approx \psi_i(\mathbf{x}). \tag{23}$$

Please note that at this point nothing can really be said or inferred about the relationship between the diffusion map transition matrix eigenvalues and the exact generator or propagator eigenvalues.

Choice of a distance metric

The LSDMap algorithm has been tested extensively and has been applied to study the free energy landscape of a number of molecular systems.[16,33,36,38,39] The use of a constant localscale as proposed in the original formulation[56] was found to be inadequate for MD data, as thoroughly discussed in the references above. Another crucial choice in LSDMap is the definition of the metric distance involved in the diffusion kernel (20). Similarly, the choice of a suitable distance is a key ingredient for kinetic clustering protocols in the definition of kinetic models such a MSMs. In the diffusion map scenario, the prescription to compute distances influences the definition of diffusion distance preserved upon projection; in the MSMs, it is fundamental to discretize the configuration space, lump similar configurations together and separate dissimilar ones, making sure that slow- interconverting states are distinguished and well separated.

Standard choices for distance metrics for molecular systems, such as the Root Mean Square Deviation, RMSD, generally use static information from each configuration to define structural similarity. However, it has been shown in a number of publications[57,58] that kinetic similarity (that is, how long it takes for a configuration to evolve into another) is crucial in the definition of distance relationship between the molecular configurations. Metric distances based on purely geometrical criteria suffer when slow conformational transitions between geo-

metrically proximal states exist, such as register shift dynamics in β-sheet protein topologies, or, in general, geometrically similar states separated by large free energy barriers.

A general and transferrable protocol to design alternative concepts of metric distances accounting for the interplay between structural and kinetic similarity is lacking. A first step towards this direction would be to compare and contrast the performance of different structural metric distances. It was shown[50,57,58] that different geometrical metrics capture kinetic properties in a specific, metric-dependent fashion. Here we contribute to this discussion by using the variational principle to decide between different choices of metric distances, in that it provides us with a quantitative tool to assess the performance of each metric in the context of LSDMap.

Methods

Fip35 setup and simulation

WW domains are small, independently folding protein domains that bind to proline-rich sequences. Their topology is characterized by two β hairpins, which form a three-stranded β-sheet. A number of mutants of the 35 amino acids WW domain of the human protein Pin1 have been engineered which fold in few tens of microseconds,[59] the fastest of them being the Fip35 mutant. The mutants small size and their ultrafast kinetics make them ideal benchmark systems, for which numerical simulations can be compared to a large body of experiments.

Recently, D.E. Shaw research group has generated two 100 μs Fip35 trajectories using the AMBER99SB-ILDN all-atom force field in TIP3P explicit water, at 337 K using a Nose-Hoover thermostat with a relaxation time of 1.0ps.[2] This dataset is used here as the equilibrium sampling onto which multiple Variational Diffusion Map calculations were performed. The setup details are given below.

LSDmap setup

The LSDMap analysis was repeated for different choices of distance metrics and different choices for the local scale parameter ϵ in order to assess to what extent the algorithm performance is affected.

Four choices of distance metrics were considered: three of them (RMSD, DD, CMD) have an immediate structural interpretation in terms of simple physical degrees of freedom; the other metric (KD) is less intuitive and requires a more detailed discussion.

Structural metrics: RMSD, DD, CMD

Let $\mathbf{x}^\alpha$ and $\mathbf{x}^\beta$ be any two molecular configurations. Their mutual Root Mean Square Deviation (RMSD) is defined as

$$\mathrm{RMSD}(\mathbf{x}^\alpha, \mathbf{x}^\beta) = \sqrt{\frac{1}{N}\sum_i (x_i^\alpha - x_i^\beta)^2} \tag{24}$$

where the sum runs over the N heavy atoms. The two configurations have to be preliminarly aligned in an optimal way such that their Euclidean distance is minimized.

Inspired by the discussion in Cossio *et al.*,[57] we considered two additional structural metrics, the dihedral and the contact map distance. The Dihedral Distance (DD) is defined as

$$\mathrm{DD}(\mathbf{x}^\alpha, \mathbf{x}^\beta) = \sqrt{\frac{1}{M}\sum_i \frac{1}{2}\left(1 - \cos\left(\varphi_i(\mathbf{x}^\alpha) - \varphi_i(\mathbf{x}^\beta)\right)\right)} \tag{25}$$

where the set of M dihedrals $\{\varphi_i\}$ formed by the backbone atoms N, C_α, C, N is considered. As a reduced number of degrees of freedom is used to measure distances with the DD metric, it is expected to perform faster than rmsd and it is an appealing candidate for heavy-duty computations, such as biased MD.[39]

The Contact Map Distance (CMD) is defined as a standard Euclidean distance in the

space of heavy atom contacts

$$\mathrm{CMD}(\mathbf{x}^{\alpha}, \mathbf{x}^{\beta}) = \sqrt{\frac{1}{N^{\alpha\beta}} \sum_{i \neq j} (C_{ij}(\mathbf{x}^{\alpha}) - C_{ij}(\mathbf{x}^{\beta}))^2} \tag{26}$$

where $C_{ij}(\mathbf{x}) = \frac{1-(r_{ij}(\mathbf{x})/r_0)^8}{1-(r_{ij}(\mathbf{x})/r_0)^{12}}$ is a smooth definition for a contact formation, r_{ij} being the Euclidean distance between heavy atom pair $i-j$ and $r_0 = 0.35\,nm$ being an appropriate cutoff; $N^{\alpha\beta} = \sqrt{(\sum_{ij} C_{ij}^{\alpha})(\sum_{ij} C_{ij}^{\beta})}$ is a normalization constant.[57] CMD is popularly employed in bioinformatics in structure analysis, such as in structure prediction algorithms;[60] hence, it appears to be a relevant alternative to RMSD while approximately retaining the same level of coarse-graining description.

Kinetic Distance (KD)

The last metric distance considered in the analysis is a kinetic distance (KD),[61] based on the Time-lagged Independent Component Analysis (TICA).[42,43] TICA is a linear dimensionality reduction technique which builds linear combinations out of a chosen set of molecular coordinates $\{r_i(t)\}$ such as atomic positions, distances, angles, in such a way that the eigenvectors and eigenvalues of the propagator of the dynamics, $\mathcal{P}$, are approximated. A comprehensive and detailed description of the algorithm can be found in.[42] In practice, TICA performs a variational optimization as described in the Theory section. Given MD data, a set of input coordinates $\{r_i(t)\}$ is chosen and the mean-free coordinates

$$y_i(t) = r_i(t) - \langle r_i(t) \rangle_t \tag{27}$$

are defined. The y_is are then used as input basis functions χ for the variational calculation specified by equations (7)-(9). Let us denote as $\hat{\psi}_i$ and $\hat{\lambda}_i$ the approximated eigenvectors and eigenvalues respectively from the TICA calculations (at a given lag time reference value τ_{TICA}).

The dominant linear combinations span a low dimensional space where the system slowest processes live. The kinetic distance is then defined as the Euclidean distance in this space upon scaling the $\hat{\psi}_i$ by the corresponding eigenvalues in the following way[61]

$$KD(\mathbf{x}^\alpha, \mathbf{x}^\beta) = \sqrt{\sum_{i=1}^{q} \hat{\lambda}_i^2 \left(\hat{\psi}_i(\mathbf{x}^\alpha) - \hat{\psi}_i\left(\mathbf{x}^\beta\right)\right)^2} \tag{28}$$

It was shown[61] that using KD as a distance metric for clustering yields Markov State Models with better approximation qualities than when unscaled TICA coordinates are used. Moreover, the eigenvector rescaling in equation (28) weighs the TICA coordinates according to their "slowness", thus making the question of how many coordinates need to be taken into account in the clustering obsolete.

In our protocol, the input parameters $\{r_i(t)\}$ to the TICA calculations were chosen to be all the mutual C_α distances (that means, each configuration in the dataset is labelled by a list of all the mutual distances) at a lag time $\tau_{TICA} = 0.1\mu s$. It is worth pointing out that this metric distance reduces to the standard Diffusion Distance (18) if the MD dataset was generated by a reversible purely diffusive process.

The four metric distances (24)-(26) and (28), were used to run separate and independent LSDMap calculations on the Fip35 data set, by using the algorithm detailed in the Theory section. Two different choices were used for the local scale parameter $\epsilon(\mathbf{x})$ in the diffusion map kernel (20):

1. A constant value $\epsilon(\mathbf{x}) = \epsilon$, where different values of ϵ were tested (Diffusion Map)

2. The distance to $N_k(\mathbf{x})$, the kth nearest neighbor configuration to configuration $\mathbf{x}$ in the dataset:

$$\epsilon(\mathbf{x}) = ||\mathbf{x} - N_k(\mathbf{x})||^2 \tag{29}$$

The diffusion coordinates are computed as the eigenvectors of the diffusion map transition

matrix M in eq. (22). Subsequently, these coordinates were orthogonalized and used as basis set $\{\chi_i\}$ for the variational method, as described in the Theory section.

Variational optimization

Were this LSDMap approximation exact, then the stationary eigenvector $\varphi_0(\mathbf{x})$ of M would be identical to $\pi(\mathbf{x}) = \mathrm{e}^{-\beta U(\mathbf{x})}$ and then the eigenvectors would be orthonormal with respect to this density ($\langle\tilde{\psi}_i, \tilde{\psi}_j\rangle_{\varphi_0} = \langle\psi_i, \psi_j\rangle_\pi = \delta_{ij}$).

Because we assume to have some finite approximation errors, we perform an orthogonalization procedure in order to obtain self-consistent diffusion coordinates. We first compute the overlap matrix:

$$c_{ij}(0) = \langle\tilde{\psi}_i, \tilde{\psi}_j\rangle_{\varphi_0} \tag{30}$$

where $\varphi_0^\top = \varphi_0^\top M$ is the stationary eigenvector obtained from the diagonalization of the diffusion map transition matrix M. We then solve for the eigenvectors of the overlap matrix

$$\mathbf{C}(0)\hat{\psi}_i = \hat{\lambda}_i\hat{\psi}_i \tag{31}$$

and use the resulting eigenvectors

$$\chi_i = \hat{\psi}_i \tag{32}$$

as a basis in the method of linear variation described above. Note that the generalized eigenvalue problem (9) does not require the basis set to be orthogonal; however, the orthogonalization in (9) is made with respect to the stationary density of the transfer operator, while the orthogonalization in (31) is done with respect to the diffusion map stationary density. Because of the approximations involved, these orthogonalization procedures are slightly different and (30-32) is done in order to start the variational method with a self-consistent basis set.

If the diffusion coordinates were exact, $\hat{\psi}_i = \tilde{\psi}_i = \psi_i$, the variational principle correlation

matrices would be diagonal (see Eq. (10)-(13)). On the other hand, the variational principle can be used as an a posteriori validation of the approximation quality of the diffusion coordinates and to further optimize them.

Matrix elements can be computed on the fly by using a stochastic realization of the trajectory $\{x_1, x_2, \ldots, x_k, \ldots, x_T\}$. Upon orthogonalization (31), we compute the variational principle correlation matrices (7-8) as direct time averages:

$$c_{ij}(\tau) \approx \frac{1}{T-\tau}\sum_{k=1}^{T-\tau}\chi_i(x_k)\chi_j(x_{k+\tau}), \tag{33}$$

$$c_{ij}(0) \approx \frac{1}{T}\sum_{k=1}^{T}\chi_i(x_k)\chi_j(x_k). \tag{34}$$

Furthermore, we enforce the time-lagged correlation matrix to be symmetric:

$$C(\tau) = \frac{1}{2}(C(\tau) + C(\tau)^T), \tag{35}$$

then solve the eigenvalue problem (9) for different values of the lag time τ. The eigenvalues $\widehat{\lambda}_i(\tau)$ are used to approximate the kinetic timescales of the eigenprocesses, whereas the generalized eigenvectors $\{\mathbf{a}_i\}$ are the linear combination coefficients to build the approximants $\widehat{\psi}_i = \sum_{\mathbf{j}} \mathbf{a_{ij}}\chi_{\mathbf{j}}$ to the eigenvectors of the propagator.

Markov State Model

As a comparison, a Markov State Model was built on of the Fip35 dataset, using the pyEMMA package (www.pyemma.org).[62] The kinetic distance introduced above (28) was used in the definition of the MSM and 1000 k-means clusters were used as clustering protocol. It is worth pointing out that other MSM-based Fip35 studies[49,50] use metrics for clustering that are different from KD. Timescale convergence was studied and compared to varDM results and literature.

Results and Discussion

The folding of WW domain Fip35 mutant

The folding of the Fip35 mutant of the WW domain has been widely investigated. For example, MD simulations[63,64] were performed for a time interval longer than $10\mu s$ but no folding transitions were observed. Pande and coworkers[65] tackled the problem using a world wide distributed computing scheme, and found transitions proceeding through a multitude of qualitatively different and nearly equiprobable folding pathways. A very different conclusion was reached by Shaw and collaborators,[2] by analyzing ultralong MD trajectories with multiple unfolding/folding events, obtained using a special-purpose supercomputer. The authors concluded that Fip35 folds predominantly along a pathway in which the first hairpin is fully structured, before the second hairpin begins to fold. On the same line, they concluded that no relevant barriers are present in the folding process; hence, Fip35 is an incipient downhill folder.

Krivov[46] challenged this interpretation and proposed the existence of intermediates revealed by using a novel optimized reaction coordinate on the same dataset. Moreover, he proposed that an alternative folding pathway also exists, in which the second hairpin forms before the first hairpin, though it is five times less likely than the main pathway.

Markov State Model analysis[49,50] of the same Fip35 dataset also suggested that folding mechanism is heterogenous, though it was realized that the majority of the folding flux flows through the path reported by Shaw.[2] Characteristic timescales were estimated to be $5\,\mu s$, and faster processes were also investigated systematically.

Recently, Mori and Saito[48] built on the popular PCA approach to propose a Dynamic Component Analysis using temporal information from the trajectory and concluded that Fip35 is not an incipient dowhnill folder. They succeeded in identifying two misfolded states where the trajectory happens to be temporarely trapped; hence, explaining the reason for

dynamic heterogeneity.

Finally, Berezovska et al.[47] presented a network-based analysis of the same data by looking at local fluctuations of conventional order parameters such as RMSD and recapitulated previous results by showing that folding occurs along two preferential pathways, both involving intermediates formation. Their estimate for the mean first-passage folding time is $4.3\,\mu s$.

Beccara et al.[66,67] generated their own MD dataset using the DPR protocol[68] and confirmed that Fip35 folds mostly through two channels which differ in the order in which hairpins are formed, and that folding involves intermediates.

In the following we contribute to the discussion by analyzing the Fip35 dataset using the varDM hybrid approach based on LSDMap and the Variational Principle, as described above. Our analysis reveals that standard structural metrics used to define configuration similarity are not appropriate, in that they do not fully capture the kinetic properties of the system. We propose a new way of computing distances between configurations which turns out to be extremely effective, kinetically and computationally. Our results show that the Fip35 folding mostly proceeds via on-pathway intermediate(s), in qualitative agreement with previous results based on reaction coordinate optimization.

Results

Optimal LSDMap parametrization

The original data set was downsampled to $100,000$ uniformely spaced points, so that two consecutive configurations are separated by a 2 ns time interval. Multiple varDM calculations were performed using metrics (24)-(26) with both constant and adaptive localscales, as described above, and a input basis set of 100 diffusion coordinates.

The distribution of the local scale values obtained using the k-nearest neighbor definition provided in eq. (29) is bimodal (data not shown), suggesting that the definition of an appro-

priate constant ϵ value may be difficult, once again supporting the need of an adaptive, point dependent localscale.[16,39] Results for different constant localscale values are discussed in the Supporting Information.

Results obtained by using eq. (29) are very robust against varying the number of nearest neighbors k over a broad range from 5 to 10000, as showed in the left panel of Fig. (S1). This result indicates that appropriate network connectivity is ensured by an extremely small fraction of points, and that the dataset manifold shape is preserved.

In the following we will show the results obtained with $k = 2000$.

Eigenvalues and Implied Timescales

The variational eigenvalue problem (9) is solved for increasing values of the lag time τ to study the convergence of both eigenvalues and eigenvectors. In principle, both quantities are lag time independent, since the generator (14) does not depend on τ explicitly. However, in practice, some equilibration over short timescale is expected, where timescales and eigenvectors gradually converge to their asymptotic values. This can be interpreted formally by invoking theoretical results about MSM convergence, once it is realized that the variational formulation with characteristic functions as basis functions is equivalent to a MSM.[45] On the other hand, if too long of a lag time is chosen, then decorrelation time and trajectory length start being comparably long, and estimates are no longer reliable. Thus, we expect only a limited range of lag time values where physical convergence of model parameters is reached, as customarily observed.[25,42,44,45] A bootstrapping procedure was employed to estimate statistically meaningful errorbars for the timescales and the linear combination coefficients.

As pointed out in the previous section, we are discussing here optimization results obtained choosing $k = 2000$ for localscale computation. Fig. (1) shows the convergence of the first

three implied timescales associated with Fip35 kinetics,

$$t_i = -\frac{\tau}{\log \widehat{\lambda}_i(\tau)} \qquad i = 1, 2, 3 \tag{36}$$

obtained with the structural metrics and the kinetic distance metric (28) (panels a, b and c). A comparison with the Markov State Model results is showed in panel (d). The semilogarithmic scale helps highlight the improvement of convergence upon using the kinetic metric; indeed, t_1 enters its convergence region around $\tau = 0.1\,\mu s$ and $\tau = 4\,\mu s$ when kinetic distance or structural distances are used respectively (for visualization purposes, the plots are truncated). The corresponding estimate for the folding characteristic timescale is $6.2\,\mu s$ and $(5.5 \pm 2.0)\mu s$ respectively, in agreement with each other, with MSM results and other estimates obtained using alternative analysis procedures.[46–50] By invoking the variational bound, we claim that all four metrics metrics employed in the calculations provide consistent results within the errorbars in the estimation of the first timescale, though KD and CMD performing slightly better in absolute terms.

In contrast, a different scenario arises when the second timescale t_2 is considered. On one hand, KD calculations converge nicely to $t_2 \approx 1\,\mu s$; on the other hand, structural metric calculations show (see Fig. (1)) that the unphysical region is entered even before real convergence sets in, and that the process occurs on a timescale $t_2 = (60 \pm 5)ns$ which is about two orders of magnitude smaller than the folding process. According to the results obtained with the structural metrics, Fip35 kinetics displays a marked timescale separation: a μs folding process couples with faster ns eigenmotions. In addition, t_1 would converge in such a regime where higher order processes have died off already, and this poses a consistency problem. Indeed, the set of timescales should be the solution of the eigenvalue problem (9) at a well-defined lag time τ, and so it is reasonable to assume that a given range of τ exists where all timescales converge; clearly, this is not the case here.

However, KD results are much more robust, all timescales converges almost simultane-

ously, and provide a t_2 estimate which is on the microsecond timescale (panel b), mirrowing the benchmark MSM calculations (panel d).

The situation is even more critical for implied timescale t_3, which is degenerate with t_2 in RMSD, DD and CMD calculations (panel c), while is well-separated from t_2 by an order of magnitude, as MSM calculations (panel d) show and the kinetic distance setup confirms.

All in all, the timescale analysis suggests that the convergence issues and the large timescale separation $t_1 \gg t_{2,} \approx t_3$ exhibited in RMSD, CMD and DD calculations is an artifact of the structural metrics which systematically miss the second slowest process in the system dynamics. The use of purely structural metrics in LSDMap results in the systematic underestimation of the characteristic timescale associated with Fip35 processes faster than plain folding. Now we turn our attention to the optimized eigenvectors.

Optimized eigenvectors

Discussing how the optimization affects the Diffusion Coordinates allows to assess to what extent LSDMap results are reliable and whether they require any a posteriori optimization. As a visual aid to the discussion, we show the linear combination coefficient matrix $[A]_{ij} = a_{ij}$ (see eq. (6)) for each calculation setup, see Fig. (2). We took into account multiple fast processes, to better elucidate that some of those may be surprisingly important in shaping the optimized eigenvectors. Let us now briefly discuss the results qualitatively and their implications. We considered the equilibrium eigenprocess, and the first seven non trivial eigenprocesses ($m = 7$). It is worth recalling though, that the first 100 diffusion coordinates were fed to the optimization procedure; we are showing in Fig. 2 just a portion of the A matrix for the sake of clarity.

We see an optimal one to one correspondence between the variationally optimized equilibrium distribution $\widehat{\psi}_0(x)$ and LSDMap Boltzmann $DC_0(x)$ and the first non-trivial eigenvectors $\widehat{\psi}_1(x)$ and $DC_1(x)$, for any metric choice. However, this type of regularity is partially lost if higher orders are considered. Indeed, different patterns arise, which compromise the diagonal

structure of the coefficients we would expect. Off-diagonal elements become important, and RMSD and CMD are the only setups where the diagonal structure is approximately preserved even for $\widehat{\psi}_2(x)$, despite the corresponding eigenvalue being completely missed (see Fig. (1)). On the other hand, KD does not display a nice diagonal structure, in spite of the timescales being well approximated; indeed, $\widehat{\psi}_2, \widehat{\psi}_3, \widehat{\psi}_4$ all have large components along DC_3.

It is quite unexpected to see that coefficient a_{22} is exactly equal to zero in panel (d). Physically, this shows that the DC_2 direction in the subspace is practically orthogonal to the optimized $\hat{\psi}_2$ direction and indicates that LSDMap further optimization is necessary.

In conclusion, our analysis shows that LSDMap calculations equipped with structural metrics such as RMSD, DD or CMD project onto a low dimensional space systematically missing the second non trivial process, whereas a kinetic distance such as KD works very well, as comparison with MSM calculations shows. Nevertheless, bare LSDMap results can be further optimized by building optimal DC linear combinations according to the prescription (9).

Eigenvector correlations

We plotted the time evolution of the estimates $\widehat{\psi}_1, \widehat{\psi}_2$ for the four metric distances considered and their cross-correlations, to check a posteriori to what extent the results correlate with one another. Figs. (3) and (4) clearly show how $\widehat{\psi}_1$ results from all metric calculations are consistent with one another. Exactly the same transitions between the folded and unfolded state (negative and positive $\widehat{\psi}_1$ values respectively) are found in each setup, and the Pearson coefficient $\rho = 0.96$ guarantees almost perfect correlation. This is consistent with previous timescale results Fig. (1) showing that all metric distance setups nicely approximate the true folding timescale t_1 upon optimization.

The scenario is more complicated if we look at the time evolution of the second diffusion coordinate (right panel in Fig. (3)). The kinetic distance highlights a much slower process than structural metrics do, and transitions showed in the top and bottom panel do not corre-

late at all, as showed in Fig. (4b). This was expected, since structural metrics systematically miss the second eigenprocess, whereas KD metric captures it correctly.

Free energy and structure analysis

As discussed in previous sections the KD metric distance provides superior results than popular structural metrics. We now consider the free energy plot as a function of the variationally optimized KD eigenvectors in Fig. (5), and extract physical observations about the dynamics of Fip35.

There is a clear separation between the folded and unfolded state (positive and negative ψ_1 respectively), as the structural metrics also encoded. The two of them are separated by a minimum at $\psi_1 \approx 0.004$ which appears to be an intermediate (A) along the folding pathway. The presence of this state shows that folding cannot be downhill incipient, in agreement with other studies.[46–48] In addition, there is an additional basin (C) just outside the unfolded state at $\psi_1 \approx 0.007$ and a cloud of dispersed states (B) at $\psi_1 \approx 0.004$ which elongates orthogonally to the horizontal folding direction. To better investigate the features of these states, heavy atom contact maps were built on sets of structures sampled from the trajectory.

The contact map analysis reveals that the first hairpin is formed in the intermediate (A), but the second is not. This uncovers one of the two folding pathways discussed in the literature[46,47,66,67] Previous MSM models[49] also identify this pathway in the transition network as that featuring the largest probability flux. In addition, the contact map shows that states falling in (B) all share a native-like structure, though some key contacts are rearranged. In particular, the first hairpin is out-of-register. Projecting the trajectory onto the $\widehat{\psi}_1 - \widehat{\psi}_2$ plane reveals that (B) is accessed only from the unfolded state, and no directed connections exist to or from the folded state located in the bottom left of Fig. (5). Thus, state B represents a misfolded state, similar to those found in previous studies.[47,48] Finally, state (C) exhibits a random-coil structure, where the second hairpin starts being formed (a number of key contacts are being formed). Projecting productive trajectory portions onto

the free energy plot in Fig. (S2) reveals that state (C) does uncover an additional transition pathway, where hairpin 2 is formed, followed by hairpin 1 and the immediate transition to the folded state. As a reference, two sample transitions are plotted on the top of the free energy plot in Fig. (S2) the blue and red trajectory display a hairpin 1 - hairpin 2 and hairpin 2 - hairpin 1 folding events, respectively.

Conclusions

We introduced an innovative technique which combines LSDMap and the Principle of Linear Variation to extract physically meaningful collective coordinates from a molecular dynamics dataset. This formulation is particularly appealing, since it overcomes issues with both building blocks. It allows to compute information about the timescales shaping up the kinetics, which is not possible in the original classic LSDMap algorithm.

Diffusion maps themselves are limited by the fact that they assume an overdamped diffusion process in the metric space used and this may not allow the eigenfunctions of the Markov backward propagator to be represented perfectly. However, the individual diffusion coordinates do not need to be perfect approximations to the real eigenfunctions to to provide a good basis set for the variational procedure. The requirement is only that the first m backward propagator eigenfunctions (of interest) need to be well representable by the set of n diffusion coordinates used. If n goes to N (number of samples), then the basis set accuracy improves, and the systematic error reduces.

In addition, the variational approach is not limited to use one type of basis function. Diffusion coordinates can be combined with other basis functions, such as MSM characteristic functions, Gaussians, etc. The motivation for the choice of diffusion maps here is that, by experience, they usually provide good approximations to the true backward propagator eigenfunctions[33,69,70] so they are likely good basis set components in a variational approach.

We applied our variational diffusion map protocol to study the Fip35 protein with two

purposes. First of all, we were interested in assessing to what extent changing LSDMap parameters would affect the quality of the results. Hence, we adopted four complimentary and indepentent definitions of metric distance to formalize the concept of distance in the configuration space. Our calculations showed that standard structural metrics based on RMSD, dihedrals or contacts are not appropriate, and that introducing an alternative distance metric that can capture the kinetic properties at least approximately, such as TICA, significantly outperforms them. Secondly, our approach allows to characterize the slow processes in the folding dynamics of Fip35. The characteristic folding timescale calculated with our protocol is consistent with previously proposed calculations adopting alternative analysis algorithms. The analysis of free energy profiles support the intermediate folding hyphotesis previously proposed in other studies.[46–48,66,67] Additionally, an orthogonal motion involving a misfolded state was also found, consistent with previous work.[47,48]

The proposed technique is general and easily implemented.

Acknowledgements

We are grateful to D. E. Shaw Research for making their Fip35 trajectory available, and to Giovanni Ciccotti for enlightening discussions. We thank the members of Clementi group and Noé group for discussion and advice.

We acknowledge funding from the following grants: ERC starting grant 307494-pcCell and Deutsche Forschungsgemeinschaft NO 825/3-1 (FN), National Science Foundation CHE-1152344 and CHE-1265929, Welch Foundation C-1570 and EPSRC Grant No. EP/K039512/1 (CC).

Simulations were performed on the following shared resources at Rice University: DAVinCI was supported in part by the Data Analysis and Visualization Cyberinfrastructure funded by NSF under grant OCI-0959097; BlueBioU was supported in part by NIH award NCRR S10RR02950 and an IBM Shared University Research (SUR) Award in partnership with

CISCO, Qlogic and Adaptive Computing.

Supporting Information Available

Results for different values of a constant localscale, and two sample transition pathways are shown in the supplementary information. This material is available free of charge via the Internet at http://pubs.acs.org/.

References

(1) Shirts, M.; Pande, V. S. Screen Savers of the World Unite! *Science* **2000**, *290*, 1903–1904.

(2) Shaw, D. E.; Maragakis, P.; Lindorff-Larsen, K.; Piana, S.; Dror, R.; Eastwood, M.; Bank, J.; Jumper, J.; Salmon, J.; Shan, Y.; Wriggers, W. Atomic-Level Characterization of the Structural Dynamics of Proteins. *Science* **2010**, *330*, 341–346.

(3) Eastman, P.; Pande, V. S. Efficient Nonbonded Interactions for Molecular Dynamics on a Graphics Processing Unit. *J. Comput. Chem.* **2010**, *31*, 1268–1272.

(4) Harvey, M.; Giupponi, G.; Fabritiis, G. D. ACEMD: Accelerated Molecular Dynamics Simulations in the Microseconds Timescale. *J. Chem. Theory Comput.* **2009**, *5*, 1632–1639.

(5) Grand, S. L.; Goetz, A. W.; Walker, R. C. SPFP: Speed Without Compromise - a Mixed Precision Model for GPU Accelerated Molecular Dynamics Simulations. *Chem. Phys. Comm.* **2013**, *184*, 374–380.

(6) Schütte, C.; Fischer, A.; Huisinga, W.; Deuflhard, P. a Direct Approach to Conformational Dynamics Based on Hybrid Monte Carlo. *J. Comput. Phys.* **1999**, *151*, 146–168.

(7) Swope, W. C.; Pitera, J. W.; Suits, F. Describing Protein Folding Kinetics by Molecular Dynamics Simulations: 1. Theory. *J. Phys. Chem. B* **2004**, *108*, 6571–6581.

(8) Singhal, N.; Pande, V. S. Error Analysis and Efficient Sampling in Markovian State Models for Molecular Dynamics. *J. Chem. Phys.* **2005**, *123*, 204909.

(9) Noé, F.; Horenko, I.; Schütte, C.; Smith, J. C. Hierarchical Analysis of Conformational Dynamics in Biomolecules: Transition Networks of Metastable States. *J. Chem. Phys.* **2007**, *126*, 155102.

(10) Chodera, J. D.; Dill, K. A.; Singhal, N.; Pande, V. S.; Swope, W. C.; Pitera, J. W. Automatic Discovery of Metastable States for the Construction of Markov Models of Macromolecular Conformational Dynamics. *J. Chem. Phys.* **2007**, *126*, 155101.

(11) Buchete, N. V.; Hummer, G. Coarse Master Equations for Peptide Folding Dynamics. *J. Phys. Chem. B* **2008**, *112*, 6057–6069.

(12) Bowman, G. R., Pande, V. S., Noé, F., Eds. *An Introduction to Markov State Models and Their Application to Long Timescale Molecular Simulation.*; Advances in Experimental Medicine and Biology; Springer Heidelberg, 2014; Vol. 797.

(13) McGibbon, R. T.; Ramsundar, B.; Sultan, M. M.; Kiss, G.; Pande, V. S. Understanding Protein Dynamics with L1-Regularized Reversible Hidden Markov Models. Proceedings of the 31st International Conference on Machine Learning. Beijing, China, 2014.

(14) Noé, F.; Wu, H.; Prinz, J.-H.; Plattner, N. Projected and Hidden Markov Models for Calculating Kinetics and Metastable States of Complex Molecules. *J. Chem. Phys.* **2013**, *139*, 184114.

(15) Coifman, R. R.; Lafon, S.; Lee, A. B.; Maggioni, M.; Nadler, B.; Warner, F.; Zucker, S. W. Geometric Diffusions As a Tool for Harmonic Analysis and Structure Definition of Data: Diffusion Maps. *Proc. Natl. Acad. Sci. USA* **2005**, *102*, 7426–7431.

(16) Rohrdanz, M. a.; Zheng, W.; Maggioni, M.; Clementi, C. Determination of Reaction Coordinates Via Locally Scaled Diffusion Map. *J. Chem. Phys.* **2011**, *134*, 124116.

(17) Rao, F.; Caflisch, A. the Protein Folding Network. *J. Mol. Bio.* **2004**, *342*, 299–306.

(18) Noé, F.; Krachtus, D.; Smith, J. C.; Fischer, S. Transition Networks for the Comprehensive Characterization of Complex Conformational Change in Proteins. *J. Chem. Theory and Comput.* **2006**, *2*, 840–857.

(19) Muff, S.; Caflisch, A. Kinetic Analysis of Molecular Dynamics Simulations Reveals Changes in the Denatured State and Switch of Folding Pathways upon Single-Point Mutation of a -Sheet Miniprotein. *Proteins* **2007**, *70*, 1185–1195.

(20) Hegger, R.; Stock, G. Multidimensional Langevin Modeling of Biomolecular Dynamics. *J. Chem. Phys.* **2009**, *130*, 034106.

(21) Deuflhard, P.; Huisinga, W.; Fischer, A.; Schütte, C. Identification of Almost Invariant Aggregates in Reversibly Nearly Uncoupled Markov Chains. *Lin. Alg. Appl.* **2000**, *315*, 39–59.

(22) Bowman, G. R. Improved Coarse-Graining of Markov State Models Via Explicit Consideration of Statistical Uncertainty. *J. Chem. Phys.* **2012**, *137*, 134111.

(23) Yao, Y.; Cui, R. Z.; Bowman, G. R.; Silva, D.-A.; Sun, J.; Huang, X. Hierarchical Nyström Methods for Constructing Markov State Models for Conformational Dynamics. *J. Chem. Phys.* **2013**, *138*, 174106.

(24) Hummer, G.; Szabo, A. Optimal Dimensionality Reduction of Multistate Kinetic and Markov-State Models. *J. Chem. Phys. B* **2015**, in press.

(25) Prinz, J.-H.; Wu, H.; Sarich, M.; Keller, B.; Senne, M.; Held, M.; Chodera, J. D.; Schütte, C.; Noé, F. Markov Models of Molecular Kinetics: Generation and Validation. *J. Chem. Phys.* **2011**, *134*, 174105.

(26) Schütte, C.; Noé, F.; Lu, J.; Sarich, M.; Vanden-Eijnden, E. Markov State Models Based on Milestoning. *J. Chem. Phys.* **2011**, *134*, 204105.

(27) Noé, F.; Doose, S.; Daidone, I.; Löllmann, M.; Chodera, J. D.; Sauer, M.; Smith, J. C. Dynamical Fingerprints for Probing Individual Relaxation Processes in Biomolecular Dynamics with Simulations and Kinetic Experiments. *Proc. Natl. Acad. Sci. USA* **2011**, *108*, 4822–4827.

(28) E, W.; Vanden-Eijnden, E. Towards a Theory of Transition Paths. *J. Stat. Phys.* **2006**, *123*, 503–523.

(29) Metzner, P.; Schütte, C.; Eijnden, E. V. Transition Path Theory for Markov Jump Processes. *Multiscale Model. Simul.* **2009**, *7*, 1192–1219.

(30) Noé, F.; Schütte, C.; Vanden-Eijnden, E.; Reich, L.; Weikl, T. Constructing the Full Ensemble of Folding Pathways from Short Off-Equilibrium Simulations. *Proc. Natl. Acad. Sci. USA* **2009**, *106*, 19011–19016.

(31) Held, M.; Metzner, P.; Prinz, J.-H.; Noé, F. Mechanisms of Protein-Ligand Association and Its Modulation by Protein Mutations. *Biophys. J.* **2010**, *100*, 701–710.

(32) Silva, D.-A.; Bowman, G. R.; Sosa-Peinado, A.; Huang, X. A Role for Both Conformational Selection and Induced Fit in Ligand Binding by the LAO Protein. *PLoS Comput. Biol.* **2011**, *7*, e1002054.

(33) Zheng, W.; Qi, B.; Rohrdanz, M. A.; Caflisch, A.; Dinner, A. R.; Clementi, C. Delineation of Folding Pathways of a Beta-Sheet Miniprotein. *J. Phys. Chem. B* **2011**, *115*, 13065–13074.

(34) Kube, S.; Weber, M. a Coarse Graining Method for the Identification of Transition Rates Between Molecular Conformations. *J. Chem. Phys.* **2007**, *126*, 024103.

(35) Keller, B.; Prinz, J.-H.; Noé, F. Markov Models and Dynamical Fingerprints: Unraveling the Complexity of Molecular Kinetics. *Chem. Phys.* **2012**, *396*, 92–107.

(36) Zheng, W.; Qi, B.; Rohrdanz, M. a.; Caflisch, A.; Dinner, A. R.; Clementi, C. Delineation of Folding Pathways of a β-Sheet Miniprotein. *J. Phys. Chem. B* **2011**, *115*, 13065–74.

(37) Prinz, J.-H.; Chodera, J. D.; Noé, F. Spectral Rate Theory for Two-State Kinetics. *Phys. Rev. X* **2014**, *4*, 011020.

(38) Zheng, W.; Rohrdanz, M. A.; Clementi, C. Rapid Exploration of Configuration Space with Diffusion-Map-Directed Molecular Dynamics. *J. Phys. Chem. B* **2013**, *117*, 12769–76.

(39) Preto, J.; Clementi, C. Fast Recovery of Free Energy Landscapes Via Diffusion-Map-Directed Molecular Dynamics. *Phys. Chem. Chem. Phys.* **2014**, *16*, 19181–19191.

(40) Sarich, M.; Noé, F.; Schütte, C. On the Approximation Quality of Markov State Models. *SIAM Multiscale Model. Simul.* **2010**, *8*, 1154–1177.

(41) Molgedey, L.; Schuster, H. G. Separation of a Mixture of Independent Signals Using Time Delayed Correlations. *Phys. Rev. Lett.* **1994**, *72*, 3634–3637.

(42) Perez-Hernandez, G.; Paul, F.; Giorgino, T.; de Fabritiis, G.; Noé, F. Identification of Slow Molecular Order Parameters for Markov Model Construction. *J. Chem. Phys.* **2013**, *139*, 015102.

(43) Schwantes, C. R.; Pande, V. S. Improvements in Markov State Model Construction Reveal Many Non-Native Interactions in the Folding of NTL9. *J. Chem. Theory Comput.* **2013**, *9*, 2000–2009.

(44) Nüske, F.; Keller, B.; Pérez-Hernández, G.; Mey, A. S. J. S.; Noé, F. Variational Approach to Molecular Kinetics. *J. Chem. Theory Comput.* **2014**, *10*, 1739–1752.

(45) Noé, F.; Nüske, F. A Variational Approach to Modeling Slow Processes in Stochastic Dynamical Systems. *SIAM Multiscale Model. Simul.* **2013**, *11*, 635–655.

(46) Krivov, S. V. the Free Energy Landscape Analysis of Protein (FIP35) Folding Dynamics. *J. Phys. Chem. B* **2011**, *115*, 12315–12324.

(47) Berezovska, G.; Prada-Gracia, D.; Rao, F. Consensus for the Fip35 Folding Mechanism? *J. Chem. Phys.* **2013**, *139*, 035102.

(48) Mori, T.; Saito, S. Dynamic Heterogeneity in the Folding/unfolding Transitions of FiP35. *J. Chem. Phys.* **2015**, *142*, 135101.

(49) Lane, T. J.; Bowman, G. R.; Beauchamp, K.; Voelz, V. a.; Pande, V. S. Markov State Model Reveals Folding and Functional Dynamics in Ultra-Long MD Trajectories. *J. Am. Chem. Soc.* **2011**, *133*, 18413–18419.

(50) McGibbon, R. T.; Pande, V. S. Learning Kinetic Distance Metrics for Markov State Models of Protein Conformational Dynamics. *J. Chem. Theory Comput.* **2013**, *9*, 2900–2906.

(51) Gardiner, C. *Stochastic Methods: A Handbook for the Natural and Social Sciences*; Springer Series in Synergetics; Springer Berlin Heidelberg, 2009.

(52) Zhuang, W.; Cui, R. Z.; Silva, D.-A.; Huang, X. Simulating the T-Jump-Triggered Unfolding Dynamics of Trpzip2 Peptide and Its Time-Resolved IR and Two-Dimensional IR Signals Using the Markov State Model Approach. *J. Phys. Chem. B* **2011**, *115*, 5415–5424.

(53) Lindner, B.; Yi, Z.; Prinz, J.-H.; Smith, J. C.; Noé, F. Dynamic Neutron Scattering from Conformational Dynamics. I. Theory and Markov Models. *J. Chem. Phys.* **2013**, *139*, 175101.

(54) Deuflhard, P.; Weber, M. In *Linear Algebra Appl.*; Dellnitz, M., Kirkland, S., Neumann, M., Schütte, C., Eds.; Elsevier, New York, 2005, 2005; Vol. 398C; pp 161–184.

(55) Weber, M. Meshless Methods in Conformation Dynamics. Ph.D. thesis, 2006.

(56) Coifman, R. R.; Kevrekidis, I. G.; Lafon, S.; Maggioni, M.; Nadler, B. Diffusion Maps, Reduction Coordinates, and Low Dimensional Representation of Stochastic Processes. *Multiscale Model. Simul.* **2008**, *7*, 842–864.

(57) Cossio, P.; Laio, A.; Pietrucci, F. Which Similarity Measure Is Better for Analyzing Protein Structures in a Molecular Dynamics Trajectory? *Phys. Chem. Chem. Phys.* **2011**, *13*, 10421–10425.

(58) Zhou, T.; Caflisch, A. Distribution of Reciprocal of Interatomic Distances: A Fast Structural Metric. *J. Chem. Theory Comput.* **2012**, *8*, 2930–2937.

(59) Jäger, M.; Nguyen, H.; Crane, J. C.; Kelly, J. W.; Gruebele, M. The Folding Mechanism of a Beta-Sheet: The WW Domain. *J. Mol. Biol.* **2001**, *311*, 373–393.

(60) Caprara, A.; Carr, R.; Istrail, S.; Lancia, G.; Walenz, B. 1001 Optimal PDB Structure Alignments: Integer Programming Methods for Finding the Maximum Contact Map Overlap. *J. Comput. Biol.* **2004**, *11*, 27–52.

(61) Noé, F.; Clementi, C. Kinetic Distance and Kinetic Maps from Molecular Dynamics Simulation. *J. Chem. Theory Comput.* **2015**, *11*, 5002–5011.

(62) Scherer, M. K.; Trendelkamp-Schroer, B.; Paul, F.; Perez-Hernandez, G.; Hoffmann, M.; Plattner, N.; Wehmeyer, C.; Prinz, J.-H.; ; Noé, F. PyEMMA 2: A Software Package for Estimation, Validation, and Analysis of Markov Models. *J. Chem. Theory. Comput.* **2015**, *DOI: 10.1021/acs.jctc.5b00743*, XXX–XXX.

(63) Freddolino, P. L.; Park, S.; Roux, B.; Schulten, K. Force Field Bias in Protein Folding Simulations. *Biophys. J.* **2009**, *96*, 3772–3780.

(64) Freddolino, P. L.; Liu, F.; Gruebele, M.; Schulten, K. Ten-Microsecond Molecular Dynamics Simulation of a Fast-Folding WW Domain. *Biophys. J.* **2008**, *94*, L75–L77.

(65) Ensign, D. L.; Pande, V. S. the Fip35 WW Domain Folds with Structural and Mechanistic Heterogeneity in Molecular Dynamics Simulations. *Biophys. J.* **2009**, *96*, L53–L55.

(66) a Beccara, S.; Škrbić, T.; Covino, R.; Faccioli, P. Dominant Folding Pathways of a WW Domain. *Proc. Natl. Acad. Sci. USA* **2012**, *109*, 2330–2335.

(67) a Beccara, S.; Fant, L.; Faccioli, P. Variational Scheme to Compute Protein Reaction Pathways Using Atomistic Force Fields with Explicit Solvent. *Phys. Rev. Lett.* **2015**, *114*, 098103.

(68) Faccioli, P.; Sega, M.; Pederiva, F.; Orland, H. Dominant Pathways in Protein Folding. *Phys. Rev. Lett.* **2005**, *2*, 1–4.

(69) Rohrdanz, M. A.; Zheng, W.; Maggioni, M.; Clementi, C. Determination of Reaction Coordinates Via Locally Scaled Diffusion Map. *J. Chem. Phys.* **2011**, *134*, 124116.

(70) Zheng, W.; Rohrdanz, M. a.; Maggioni, M.; Clementi, C. Polymer Reversal Rate Calculated Via Locally Scaled Diffusion Map. *J. Chem. Phys.* **2011**, *134*, 144109.

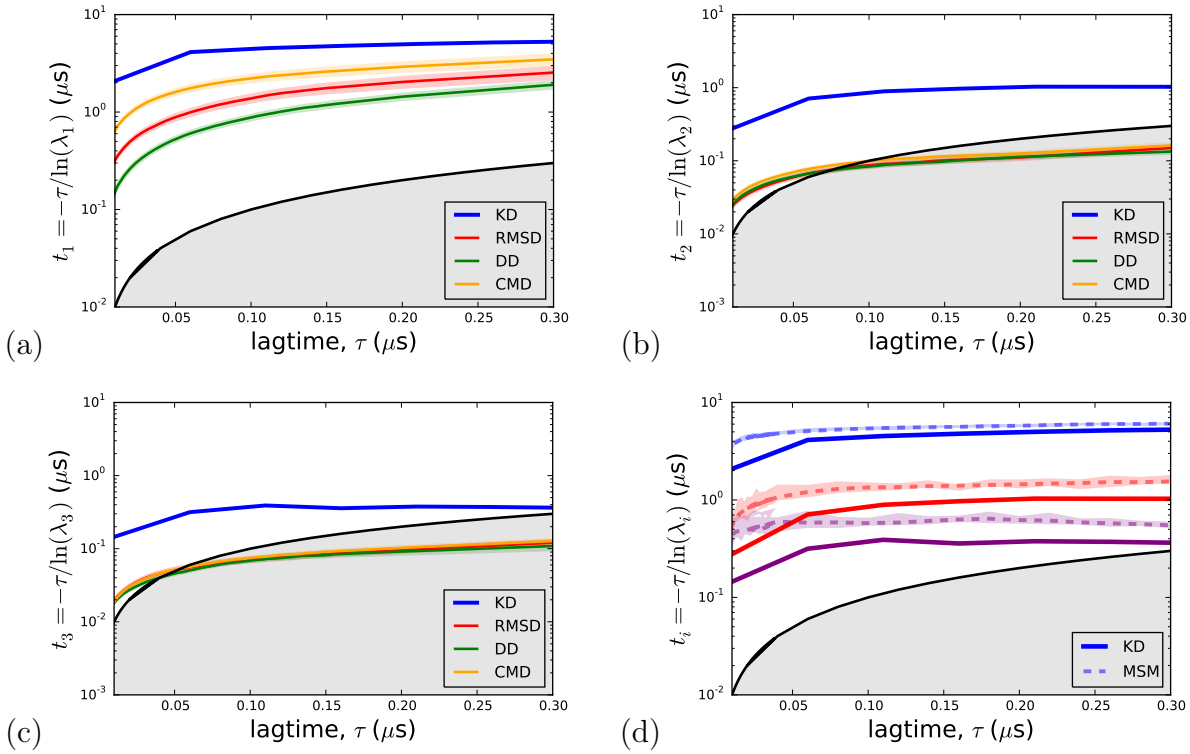

Figure 1: (a) - (c) Implied timescales t_1, t_2, t_3 as from the varDM calculations ($k = 2000$) (from panel (a), (b) and (c) respectively) using RMSD, DD, CMD, KD metric distance. All metrics are equally efficient in targeting $t_1 \approx 5.5\mu s$, even though KD estimates converge faster and almost simultaneously. The second and third implied timescales t_2, t_3 are severely underestimated by all three structural metrics considered (see panels (b) and (c)), and affected by serious convergence issues. (d) Comparison of the timescales resulting from KD varDM and MSM timescales: t_1 is blue, t_2 red and t_3 purple.

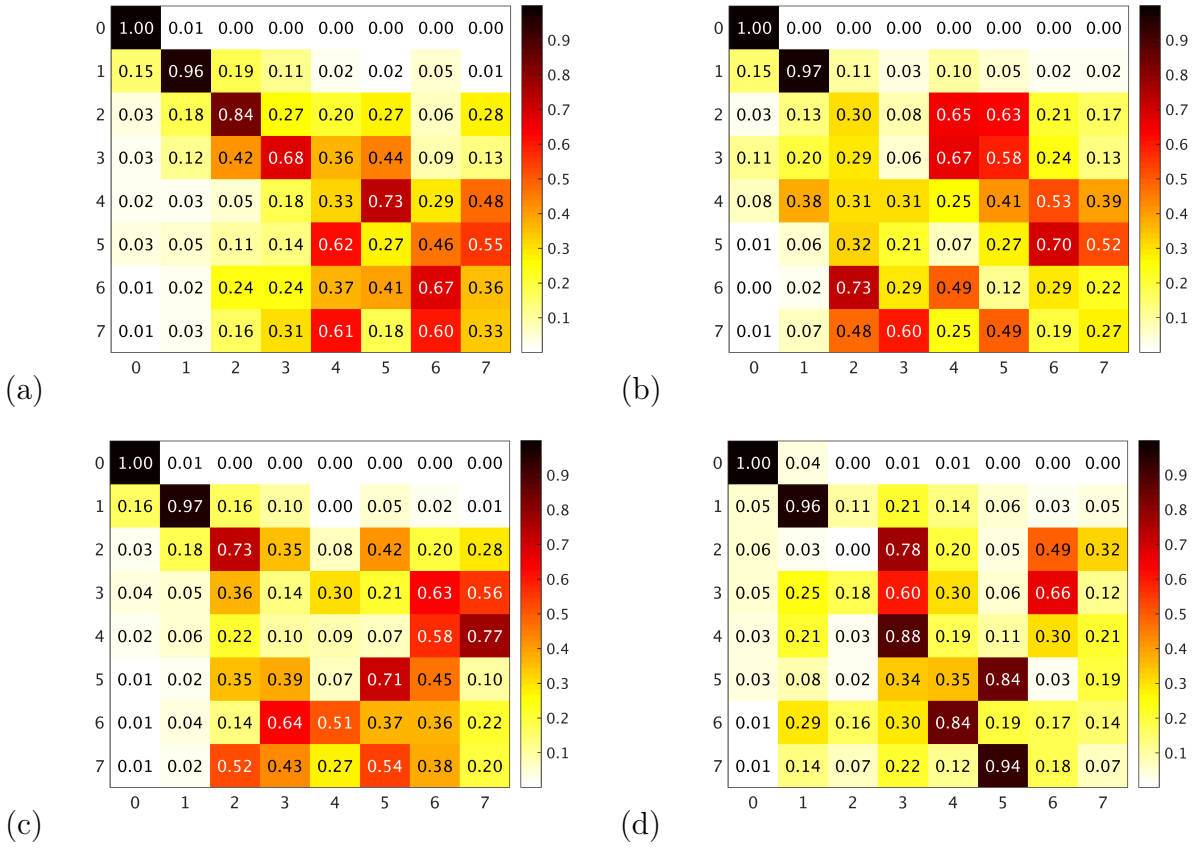

Figure 2: Truncated linear combination coefficient matrix A for RMSD (a), DD (b) and CMD (c), KD (d). The entry (i, j) is the matrix element a_{ij} and represents the component of the i-th optimized eigenvector onto the j-th LSDMap Diffusion Coordinate. Ideally we would expect an identity matrix $a_{ij} = \delta_{ij}$, but these results show that this is not the case; hence, the DCs are not invariant upon optimization.

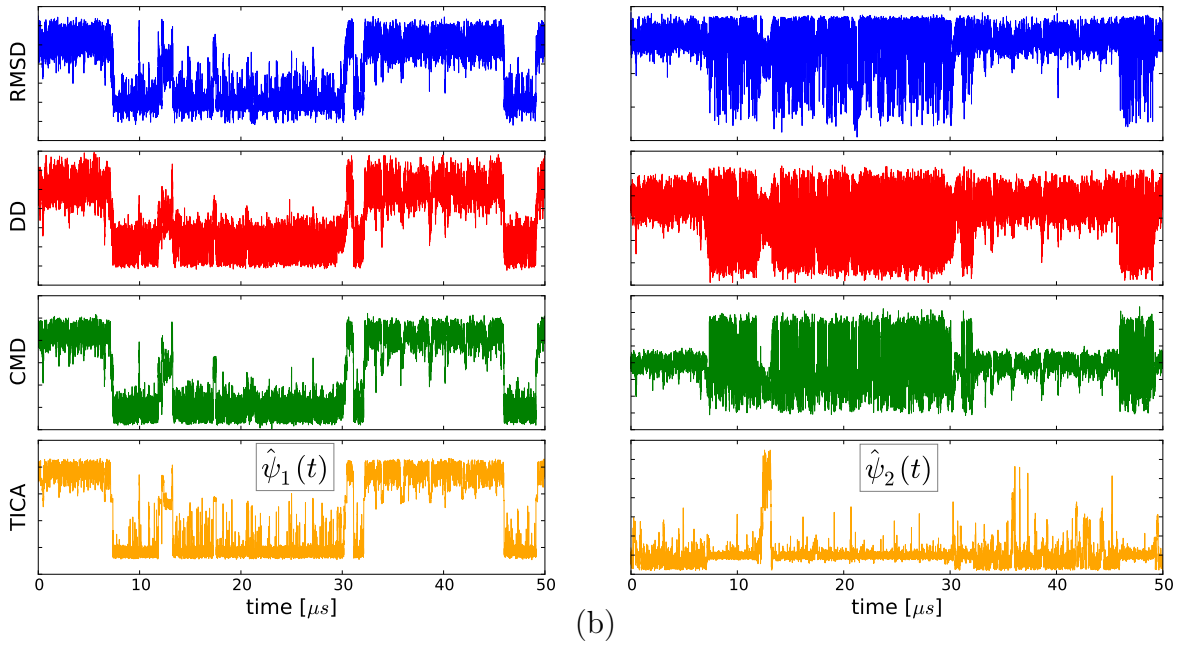

Figure 3: Time sequences for $\widehat{\psi}_1$ (panel a) and $\widehat{\psi}_2$ (panel b) from different metric calculations: RMSD (blue), DD (red), CMD (green), KD (orange), for the first Fip35 trajectory.[2] The first eigenprocess is correctly captured by all four metric choices consistently, whereas the second is not.

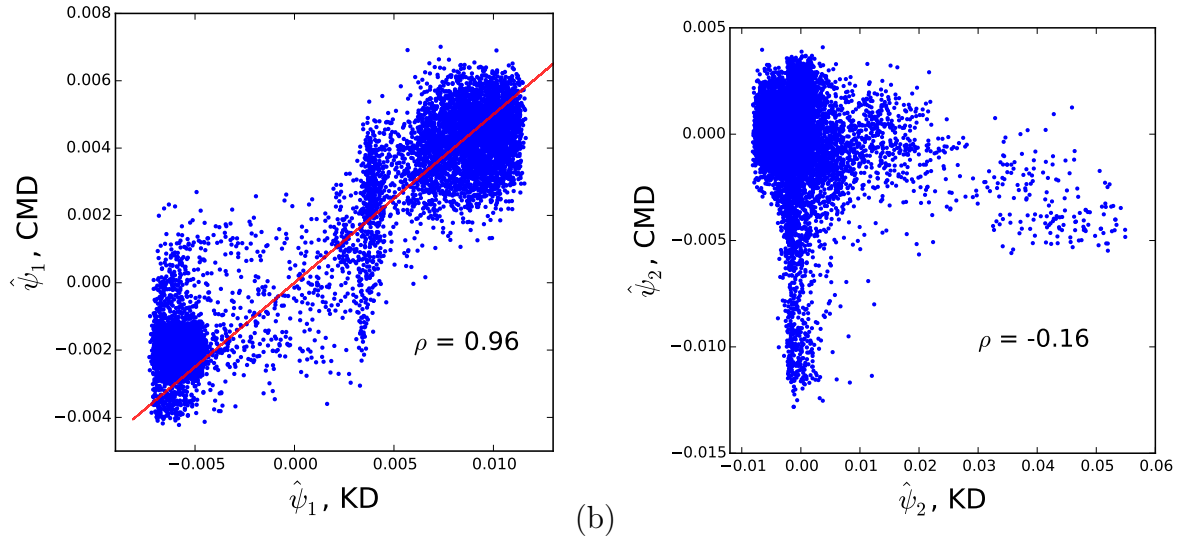

Figure 4: Statistical correlations between KD and CMD optimized eigenvectors $\widehat{\psi}_1$ (a) and $\widehat{\psi}_2$ (b). The Pearson correlation coefficient ρ is also shown.

(a)

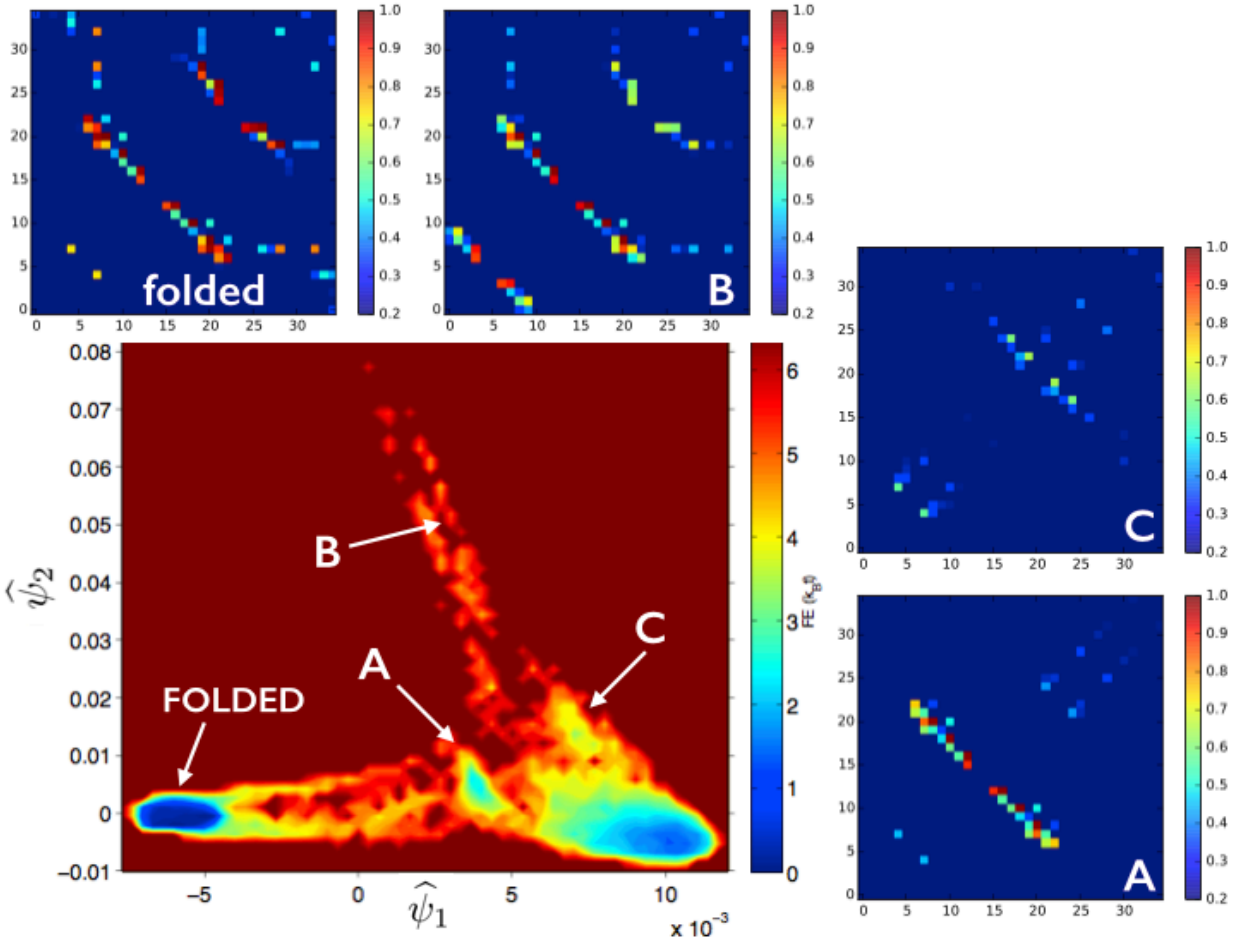

(b)

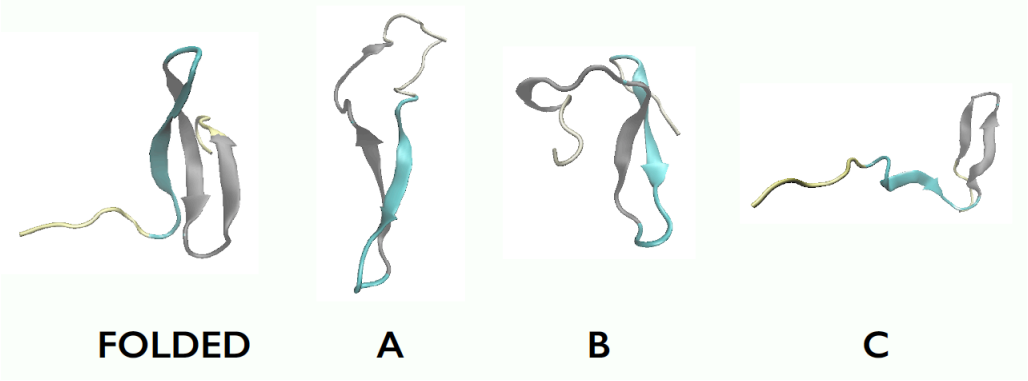

Figure 5: (a) Free energy plot as a function of the optimized KD VarDM coordinates, and sample contact maps. Folded and unfolded state are clearly separated along the $\widehat{\psi}_1$ direction; additional states are labelled (A), (B) and (C). See text for complete description. (b) Sample structures from these states.